

Improvement of microstructure, mechanical properties, and corrosion resistance of WE43 alloy by squeeze casting

Jian-cong Bian¹, Bao-yi Yu¹, Jian-fei Hao¹, Hui-wen Zhu¹, Hui-shu Wu², Bin Chen², Wei-rong Li³, Yan-fang Li³,
**Li Zheng¹, and *Run-xia Li²

1. School of Materials Science and Engineering, Shenyang University of Technology, Shenyang 110870, China

2. School of Materials Science and Engineering, Dongguan University of Technology, Dongguan 523808, Guangdong, China

3. Dongguan Eontec Co., Ltd., Dongguan 523808, Guangdong, China

Abstract: The WE43 magnesium alloy was prepared by squeeze casting, and the influence of squeeze casting parameters on mechanical properties and corrosion resistance was studied and compared with gravity casting. The gravity cast WE43 alloy shows uneven grain size distribution, and some grains even greater than 90 μm . While, the grain size of the squeeze cast WE43 alloy is mainly distributed in 20–50 μm . The $\text{Mg}_{12}\text{Nd}_2\text{Y}$ phase morphology changes from large lamellar to strips after squeeze casting, whereas Mg_{24}Y_5 phase exhibits no obvious change. The yield strength, tensile strength, and elongation of the gravity cast WE43 alloy are 127 MPa, 157 MPa, and 6%, respectively, and 145 MPa, 193 MPa, and 9.1% for squeeze cast alloy. For the squeeze cast WE43 alloy, the average corrosion rate is 0.6056 $\text{mm}\cdot\text{year}^{-1}$ according to immersion test results, and according to electrochemical measurements, the corrosion current density is 78.13 $\mu\text{A}\cdot\text{cm}^{-2}$, which is better than that of the gravity cast WE43 alloy. Compared with gravity casting, the grains and second phase of the WE43 alloy by squeeze casting are refined, and the mechanical properties and corrosion resistance are improved. This may expand the applications of the WE43 alloy.

Keywords: WE43 alloy; squeeze casting; microstructure; mechanical properties; corrosion resistance

CLC numbers: TG146.22

Document code: A

Article ID: 1672-6421(2022)05-419-08

1 Introduction

Magnesium alloys have become essential materials in aviation, automobile, computer, communication, and consumer electronics^[1-3]. Due to their excellent biocompatibility and biodegradability, numerous studies have been conducted on magnesium alloys as medical materials^[4-6]. As a biological magnesium alloy, WE43 alloy has been studied by many researchers^[7-10]. However, the properties of the untreated WE43 alloy cannot satisfy the requirement for implant materials.

Low mechanical properties and poor corrosion resistance limit the biomedical applications of magnesium alloys. How to eliminate the coarse eutectic phases and reduce the grain size of the WE43 alloy is the key to improve the properties. Extrusion^[11-13] and rolling^[14, 15] can significantly refine the microstructure and improve properties of WE43 alloy, but this improvement is limited due to the poor plasticity of WE43 alloy. Therefore, casting process, with characteristics of small deformation force, attracts many attentions.

Squeeze casting method combines the characteristics of gravity casting and plastic processing. It can cast parts with complex shapes without multiple processes^[16-18]. Compared with gravity cast magnesium alloys, squeeze cast magnesium alloys have finer grains and higher mechanical properties^[18-20]. Han et al.^[19] reported that the grains of the squeeze-cast AZ91D alloy were remarkably refined with increasing applied squeeze casting pressure. When the applied pressure increased to 100 MPa, the Mg matrix and lamellar eutectic structure were refined, and the optimal mechanical properties were obtained. Furthermore, the porosity

*Run-xia Li

Professor. Her research interests mainly focus on the heat treatment strengthening process cast Al alloys, and design of new biomedical Mg alloys.

E-mail: runxiali@163.com

**Li Zheng

Associate Professor. His research interests mainly focus on the plastic deformation and processing of light alloys.

E-mail: zhengli_1115@163.com

Received: 2021-09-26; Accepted: 2022-03-22

in squeeze cast magnesium alloys was reduced and the mechanical properties were improved compared to gravity cast magnesium alloys [21, 22].

Squeeze casting technology is widely used for magnesium alloys. However, research on the squeeze casting of WE43 alloys is limited, and the effect of squeeze casting on corrosion resistance is rarely reported. In this study, WE43 alloy was prepared via squeeze casting, and its microstructure, tensile properties and corrosion resistance were analyzed. The mechanism to improve the tensile properties and corrosion resistance of the WE43 alloy by squeeze casting was also discussed, so as to expand the applications of biomagnesium alloys.

2 Experimental procedure

Commercial WE43 ingots were used for experiments. Table 1 presents the composition of the WE43 alloy. The commercial WE43 ingots were melted at 720 °C with the protective gases of N₂ (98vol.%) and SF₆ (2vol.%) in an electric resistance furnace. Then, samples with 80 mm in diameter and 150 mm in length were prepared under squeeze casting pressure of 660 MPa, the holding time of 60 s, and die temperature of 300 °C. A gravity cast alloy was also prepared under the same conditions except for without pressure.

Table 1: Chemical composition of WE43 alloy (wt.%)

Y	Nd	Gd	Zr	Fe	Si	Cu	Ni	Mg
4.090	2.410	1.140	0.560	0.006	0.005	0.005	0.010	Bal.

Tensile specimens were prepared by following the GB/T 228.1-2010 standard. The strain rate of the room-temperature tensile test was 0.02 mm·min⁻¹. The sample for microstructure characterization was 10 mm×10 mm×10 mm. After the sample was ground and polished, it was etched using a solution containing 1 mL of acetic acid, 0.5 g of picric acid, 1 mL of H₂O, and 7 mL of ethanol. The microstructure, tensile fracture, and corrosion surface morphology of the sample were characterized using S-3400N scanning electron microscopy (SEM). Electron backscatter diffraction (EBSD) samples were ground to 80 μm. Then, the samples were treated with ion thinning. The grain size and structure were analyzed using ZEEIES Gemini 300 SEM. An XRD-7000 X-ray diffractometer was used for phase constitution analysis, at the scanning range of 20°–80° with a rate of 2°·min⁻¹.

The weight loss and pH of the sample were tested in Hank's solution [23] at 37 °C. A 10 mm×10 mm×10 mm sample cube was used for weight loss and pH experiments, and after polishing, the sample was subjected to ultrasonic cleaning. The corrosion test (ASTM G31-72 [24]) was performed with the ratio of Hank's solution volume to sample surface area is 30 mL·cm⁻². The initial pH of Hank's solution was set to 7.4. In the pH experiment, Hank's solution was not changed, whereas in the weight loss experiment, Hank's solution was replaced every 24 h. For the weight loss experiment, the sample was removed from the

Hank's solution after 192 h, washed with chromic acid (200 g·L⁻¹ CrO₃+10 g·L⁻¹ AgNO₃), and weighed on an electronic balance. The corrosion rate R_w (mm·year⁻¹) was obtained using Eq. (1) [25]:

$$R_w = \frac{K \times W}{A \times T \times D} \quad (1)$$

where constant $K=8.76 \times 10^4$, W is the weight loss (g), A is the area of the sample exposed to the solution (cm²), T is the immersion time (h), and D is the density of the material (g·cm⁻³). A pH meter was used to record the pH at different time intervals. The electrochemical experiment was performed in Hank's solution at 37±0.5 °C by using an electrochemical workstation (VSP-300, China), and electrochemical impedance spectroscopy (EIS), and the potentiodynamic polarisation (PDP) curves were analyzed. The EIS measurement frequency was from 100 kHz to 10 MHz, and the perturbation amplitude was 5 mV. The scan rate of the PDP curve was 1.0 mV·s⁻¹, and the fixed value range was -3 to 0 V.

3 Results and discussion

3.1 Microstructure analysis

Figure 1 presents the XRD results of the WE43 alloy. Both the gravity and squeeze cast WE43 alloys comprise α-Mg, Mg₂₄Y₅, and Mg₁₂Nd₂Y phases, but the intensity of the diffraction peak of the Mg₁₂Nd₂Y phase decreases, and the full width at half maximum of the (10 $\bar{1}$ 0), (0002), (10 $\bar{1}$ 1), (10 $\bar{1}$ 2) and (11 $\bar{2}$ 0) crystal plane diffraction peaks of the Mg matrix increases in squeeze cast alloy.

Figure 2 shows the microstructure of the WE43 alloy. The second phase of the gravity cast WE43 alloy is mainly the lamellar phase at the grain boundary [Fig. 2(b)]. The energy dispersive X-ray spectroscopy (EDS) analysis reveals the dot phase consists of Mg and Y elements, and the lamellar phase at the grain boundary comprises Mg, Y, and Nd. Combined with the XRD results, the dot and lamellar phases are Mg₂₄Y₅ and Mg₁₂Nd₂Y, respectively. The Mg₁₂Nd₂Y phase shows a needle-like eutectic structure [Figs. 2(a) and (b)]. Figures 2(c) and (d) present the microstructure of the squeeze cast WE43 alloy. The strip or blocky Mg₁₂Nd₂Y phases are uniformly distributed along the grain boundary, and a few Mg₂₄Y₅ phases exist inside the grains.

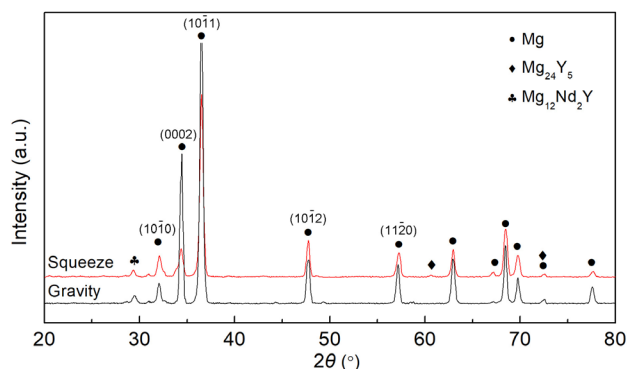


Fig. 1: XRD results of gravity and squeeze casting WE43 alloys

During squeeze casting, the pressure applied to the molten WE43 alloy affects the solute diffusion coefficient, grain growth rate, solution surface tension, and nucleation rate of the alloy [17]. After squeeze casting, the morphology of the $Mg_{12}Nd_2Y$ phase changes from large lamellar to strips. Some elements dissolve into the α -Mg matrix under pressure. Moreover, some Y and Nd elements are pushed to the grain boundary. The eutectic transformation occurs at the grain

boundary, and numerous fine strips of the $Mg_{12}Nd_2Y$ phase form at the grain boundary.

Figure 3 shows the EBSD maps and grain size distribution of the WE43 alloy. The gravity cast WE43 alloy exhibits uneven grain distribution and some grains even with a size greater than 90 μm ; the average grain size is 42 μm . The grain size distribution of the squeeze cast WE43 alloy is more concentrated, with an average grain size of 36 μm .

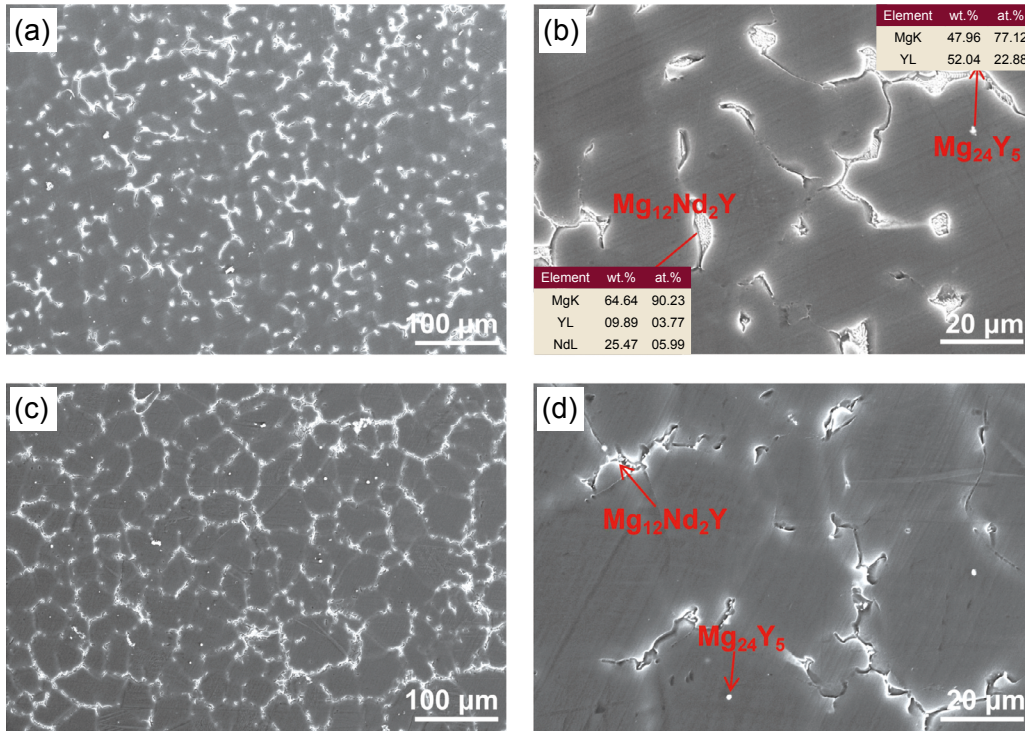


Fig. 2: Microstructures of WE43 alloy by gravity casting (a and b) and squeeze casting (c and d)

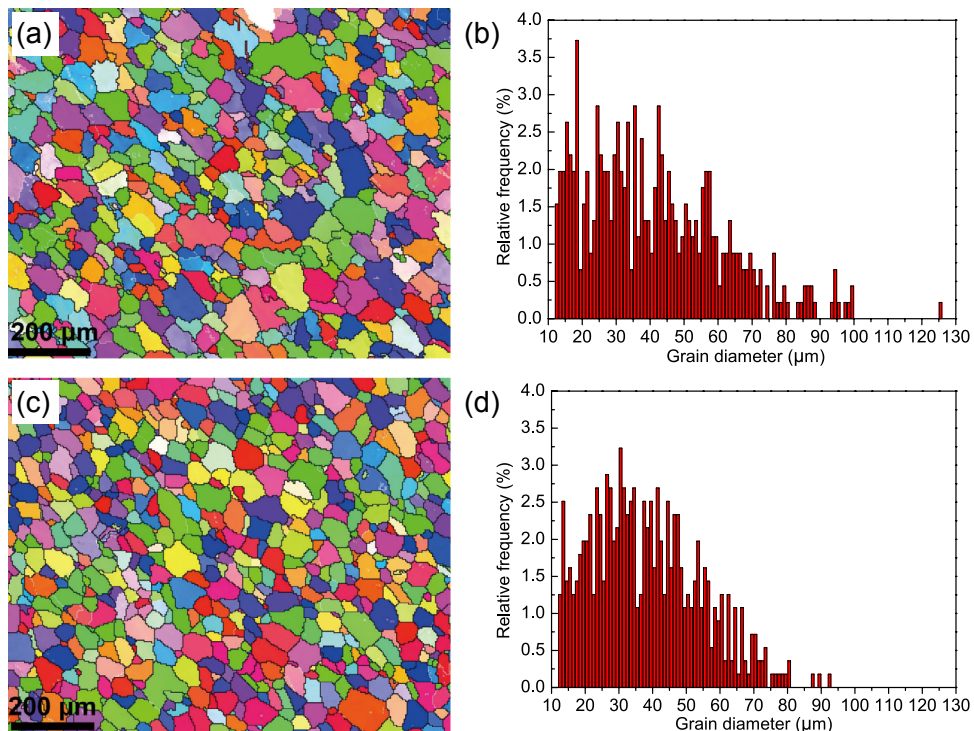


Fig. 3: EBSD maps (a, c) and grain-size distribution (b, d) of WE43 alloy: (a), (b) gravity cast; (c), (d) squeeze cast

According to Fig. 3, the grains of the alloy by squeeze casting are finer than gravity casting. External pressure changes the heat transfer mechanism of the alloy during solidification [26]. Under the gravity casting conditions, an air gap easily forms between the molten metal and mould, which leads to a decrease in the heat transfer effect during solidification and a decline in the solidification rate. While, during the solidification process in squeeze casting, due to the pressure applied, the molten metal comes in close contact with the mould, which leads to a decrease in the air gap, an increase in the heat transfer coefficient, and the acceleration of the solidification rate, and therefore the refinement of the grains [26]. When a metal liquid is under pressure, the solid and liquid states of the metal satisfy the Clausius-Clapeyron Eqs. [27]:

$$dT/dP = T(V_L - V_S)/Q \quad (2)$$

$$\Delta T = T(V_L - V_S)\Delta P/Q \quad (3)$$

where T is the melting point of the metal ($^{\circ}\text{C}$), V_L is the liquid metal volume per unit mass ($\text{cm}^3 \cdot \text{g}^{-1}$), V_S is the solid metal volume per unit mass ($\text{cm}^3 \cdot \text{g}^{-1}$), Q is the latent heat of fusion ($\text{J} \cdot \text{g}^{-1}$), ΔP is the specific pressure (MPa), and ΔT is the change in the melting point of the metal under pressure ($^{\circ}\text{C}$). The liquid-solid volume shrinkage rate of magnesium is 4.2%, its latent heat of fusion is $368 \text{ kJ} \cdot \text{kg}^{-1}$, and its melting point under standard atmospheric pressure is $650 \text{ }^{\circ}\text{C}$ [28]. In this study, the specific pressure was 660 MPa. According to Eq. (3), the melting point of the WE43 alloy increases by approximately $48.96 \text{ }^{\circ}\text{C}$. In general, the undercooling of the melt increases with an increase in the melting point, and the increase in undercooling leads to the decline in alloy nucleation work, which promotes $\alpha\text{-Mg}$ nucleation and grain refinement. In addition, pressure can increase the diffusion activation energy of solute atoms, reduce the diffusion rate of atoms, and inhibit the growth of nuclei. The decrease in the growth rate of crystal nuclei and the increase in the nucleation rate together result in grain refinement, thus, the grains of the squeeze cast WE43 alloy are refined.

3.2 Mechanical properties

Figure 4 presents the stress-strain curves of the WE43 alloys by gravity and squeeze casting, respectively. The gravity cast WE43 alloy has lower strength and plasticity; its yield strength,

tensile strength, and elongation are 127 MPa, 157 MPa, and 6%, respectively. The tensile properties of the squeeze cast WE43 alloy are improved to 145 MPa, 193 MPa, and 9.1%, increased by 14.2 %, 22.9 % and 51.7%, respectively.

Figure 5 shows the tensile fracture morphologies of the alloy by gravity and squeeze casting. Many cleavage platforms as well as a few dimples and tear edges are observed in the gravity cast WE43 alloy; the area of the cleavage platform is large, indicating that brittle fracture plays a dominant role in the fracture of gravity cast WE43 alloy. The squeeze cast WE43 alloy shows a mixture of numerous dimples and tearing edges, and a few cleavage platforms; the fracture characteristics of brittleness and ductility is observed.

Figure 6 shows the fracture of the second phase near the tensile fracture of the gravity cast WE43 alloy. Many fractured second phases can be observed near the fracture in Fig. 6(a); the magnified figure of Fig. 6(b) shows that the fractured second phase is $\text{Mg}_{12}\text{Nd}_2\text{Y}$, the Mg_{24}Y_5 phase is not fractured. During the tension process, the hard brittle $\text{Mg}_{12}\text{Nd}_2\text{Y}$ phase acts as the source of crack. As the tension progresses, the cracks propagate and connect each other, and finally, the alloy fractures.

The squeeze cast WE43 alloy has high strength and elongation mainly due to the grain refinement and $\text{Mg}_{12}\text{Nd}_2\text{Y}$ second-phase reduction (Figs. 2 and 3). The reduction of shrinkage and porosity also can improve the tensile properties [18]. In addition, squeeze casting increases the dislocation density of the sample, which leads to the improvement of strength [29]. The Dunn formula can be used to calculate the dislocation

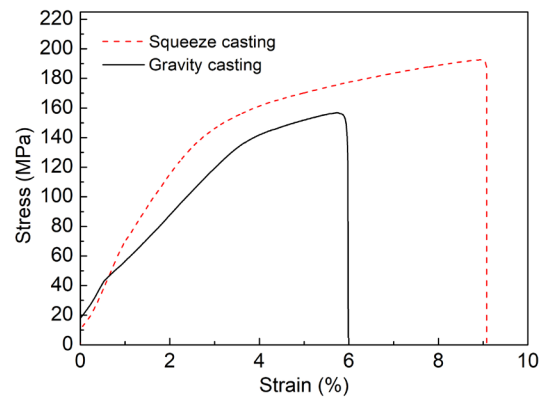


Fig. 4: Stress-strain curves of the alloy by squeeze and gravity casting

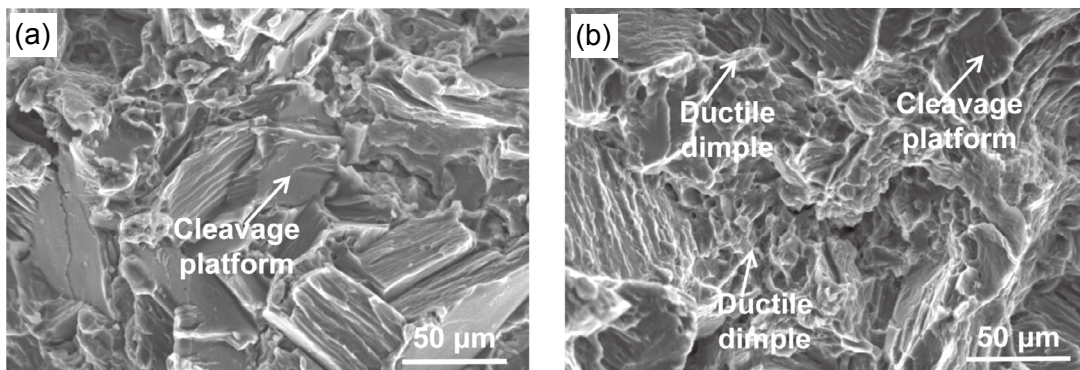


Fig. 5: Tensile fracture morphology of WE43 alloy by gravity casting (a) and squeeze casting (b)

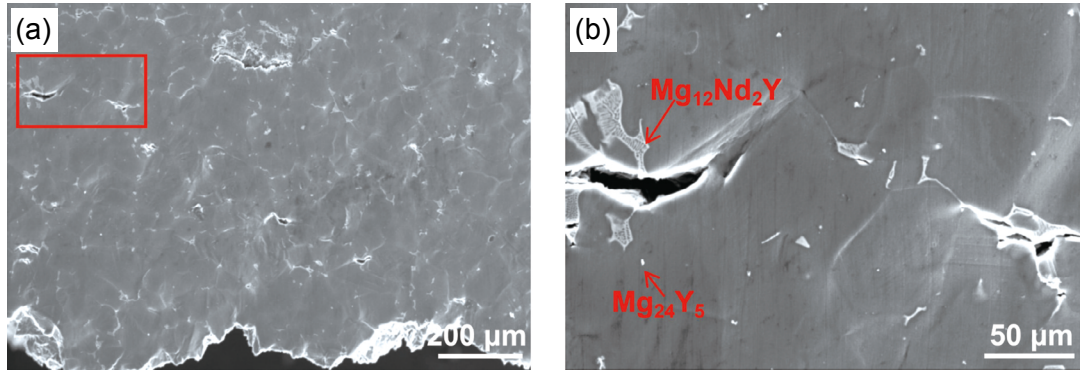


Fig. 6: Microstructure near the tensile fracture of gravity cast WE43 alloy (a), and enlargement of the box area in (a) (b)

density of the alloy^[30]:

$$\rho = \frac{L^2}{4.35 \times b^2} \quad (4)$$

where ρ is the dislocation density (cm^{-2}), L is the full width at half maximum (rad), and b is the Burgers vector. Table 2 lists the L of the main crystal plane diffraction peaks calculated using Jade software from the XRD data. The L of $(10\bar{1}0)$, (0002) , $(10\bar{1}2)$ and $(11\bar{2}0)$ diffraction peaks increases after squeeze casting, and according to Eq. (4), the dislocation density increases, and therefore the strength of squeeze cast WE43 alloy increases, which is consistent with the literature^[29].

Table 2: Full width at half maximum of the main crystal plane diffraction peaks of Mg matrix (rad)

Alloys	$(10\bar{1}0)$	(0002)	$(10\bar{1}1)$	$(10\bar{1}2)$	$(11\bar{2}0)$
Gravity cast	0.451	0.493	0.441	0.373	0.414
Squeeze cast	0.472	0.550	0.465	0.437	0.521

3.3 Corrosion resistance

Figure 7 shows the average corrosion rate of the WE43 alloy. The average corrosion rates of the gravity and squeeze cast WE43 alloys are 1.4135 and 0.6056 $\text{mm}\cdot\text{year}^{-1}$, respectively. Squeeze casting considerably improves the corrosion resistance.

Figure 8 shows the pH of the WE43 alloy at different times. The pH value initially increases sharply with an increase in the immersion time, then increases slowly, and finally, attains a nearly stable state. The pH value of the squeeze cast alloy is lower than that of the gravity cast alloy. The final pH of the squeeze cast WE43 alloy is 11.05. Under the same conditions, pH is directly related to alloy corrosion^[31]. During initial 20 h, the rapid increase in pH is caused by Mg matrix corrosion, which leads to the generation of a large amount of $\text{Mg}(\text{OH})_2$ and the increase in the OH^- content in the solution. As the immersion time increases (26–122 h), Cl^- present in the solution continues to react with $\text{Mg}(\text{OH})_2$ to form a magnesium salt, which is soluble in the solution, and pH continues to increase. However, with the accumulation of corrosion products on the sample surface, the corrosion rate decreases, and thus, increase of pH becomes slowly. With

the further increase in the immersion time (122–196 h), OH^- gradually attains a dynamic equilibrium, the pH value barely changes and becomes stable^[32].

The corrosion products of the gravity cast WE43 alloy were analyzed through XRD and EDS (Fig. 9). The EDS analysis was performed on the flaky and blocky corrosion products [Points A and B in Fig. 9(a)], and corrosion product layers (Point C) on the sample surface. According to the XRD results, C, Mg, P, O, and Ca can be observed in the energy spectrum of the corrosion products. Therefore, the corrosion products are $\text{Mg}(\text{OH})_2$, HA and $(\text{Ca},\text{Mg})_3(\text{PO}_4)_2$. HA is hydroxyapatite $[\text{Ca}_{10}(\text{PO}_4)_6(\text{OH})_2]$, which is the main component of human bones.

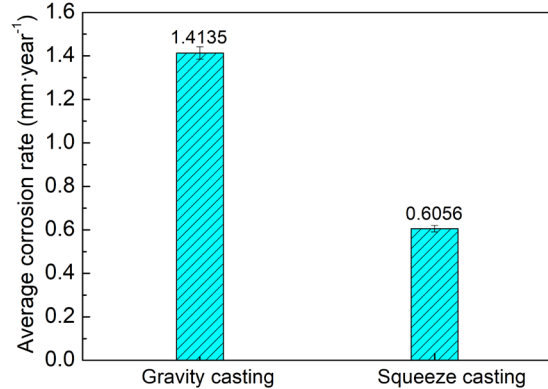


Fig. 7: Average corrosion rate of the alloys by gravity and squeeze casting, respectively

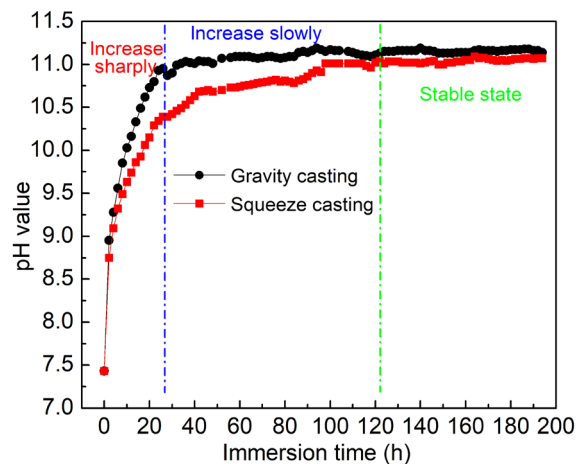


Fig. 8: Variation in pH value of WE43 alloy

The gravity cast WE43 alloy exhibits many white corrosion products, and numerous spherical corrosion product particles [Fig. 10(a)]. The squeeze cast WE43 alloy shows fewer corrosion products than the gravity cast WE43 alloy and has some uncorroded areas [Fig. 10(b)], indicating the squeeze cast alloy has higher corrosion resistance.

The gravity cast WE43 alloy after pickling shows uneven

corrosion, and many large corrosion holes are found on the surface [Fig. 10(c)]. Simultaneously, dot- and ravine-like corrosion morphologies appear along the grain boundary, and the corrosion pits are deep. Corrosion proceeds along the grain boundary. On the contrary, small corrosion holes are observed on the corrosion surface of the squeeze cast WE43 alloy. These corrosion holes are shallow, and the corrosion area is small [Fig. 10(d)].

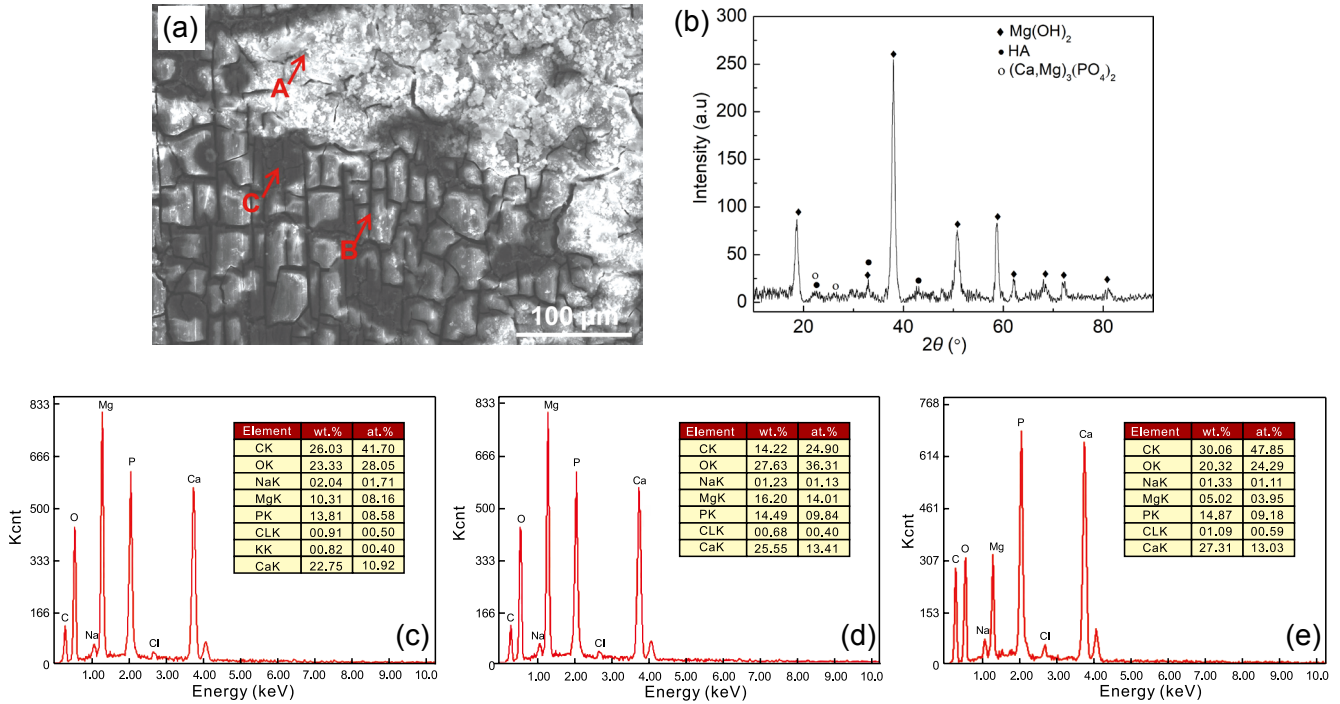


Fig. 9: Corrosion products of gravity cast WE43 alloy (a) and their XRD results (b), EDS of Points A (c), B (d) and C (e)

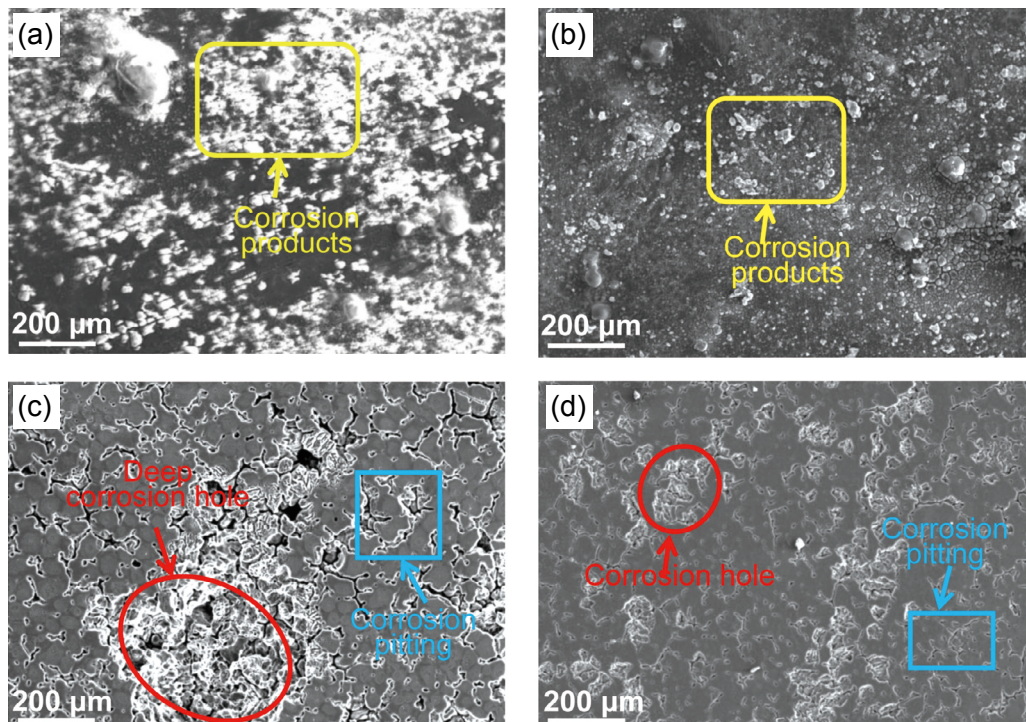


Fig. 10: Corrosion surface morphologies of WE43 alloy: (a) gravity cast sample before pickling; (b) squeeze cast sample before pickling; (c) gravity cast sample after pickling; (d) squeeze cast sample after pickling

Figure 11 shows the EIS of the WE43 alloy. In addition to different diameters, the alloy exhibits a single capacitor ring. Studies have indicated that the high-frequency capacitive semicircle reflects the charge transfer ability. The larger the radius of the high-frequency capacitive semicircle, the greater the substrate hindrance to the charge transfer during the reaction, and the higher the impedance [33]. Makar et al. [34] proposed the relationship between the diameter of EIS curve and corrosion rate of the alloy, that is, the curve diameter can indicate the corrosion resistance of the alloy. The smaller the diameter, the faster the corrosion rate and the worse the corrosion resistance of the alloy. The squeeze cast WE43 alloy has a considerably larger diameter, and therefore, its corrosion resistance is higher.

Figure 12 presents the PDP curves of the WE43 alloy. The cathodic polarisation curve shows the hydrogen evolution reaction of the alloy. The hydrogen evolution current density of the squeeze cast alloy is small. The corrosion potential E_{corr} and corrosion current density i_{corr} of the alloy can be obtained using the Tafel extrapolation method, and the corrosion rate P_i ($\text{mm}\cdot\text{year}^{-1}$) is calculated by [35]:

$$P_i = 22.85i_{corr} \quad (5)$$

The values of E_{corr} , i_{corr} and P_i are shown in Table 3. The corrosion current density of the gravity cast WE43 alloy is $183.67 \mu\text{A}\cdot\text{cm}^{-2}$, while the squeeze cast WE43 alloy offers a lower corrosion current density of $78.13 \mu\text{A}\cdot\text{cm}^{-2}$, indicating

Table 3: Fitting results of polarization curves of WE43 alloys

Alloys	Corrosion potential E_{corr} (V)	Current density i_{corr} ($\mu\text{A}\cdot\text{cm}^{-2}$)	P_i ($\text{mm}\cdot\text{year}^{-1}$)
Gravity cast WE43	-1.57	183.67	4.196
Squeeze cast WE43	-1.74	78.13	1.785

the higher corrosion performance than the gravity cast alloy. According to Eq. (5), the corrosion rate, P_i , is directly proportional to the current density, i_{corr} [36]. The average corrosion rates, P_i , of the gravity and squeeze cast WE43 alloys calculated using Eq. (5) are 4.196 and $1.785 \text{ mm}\cdot\text{year}^{-1}$, respectively.

From the results of the weight-loss and electrochemical experiments, the squeeze cast WE43 alloy exhibits higher corrosion resistance compared to gravity casting. The squeeze cast WE43 alloy has fine grains and a high grain boundary density. The finer the grains, the higher the energy of the grain boundary, which is conducive to protective film formation [37]. Thus, the squeeze cast WE43 alloy has high corrosion resistance. The reduction in the size of the coarse second phase inhibits micro-galvanic corrosion between the substrate and second phase, lowers the corrosion current density, and promotes the uniform distribution of the galvanic corrosion current on the anode surface, thereby suppressing local corrosion. In addition, squeeze casting reduces porosity and inherent defects, which is benefit to improvement of corrosion resistance.

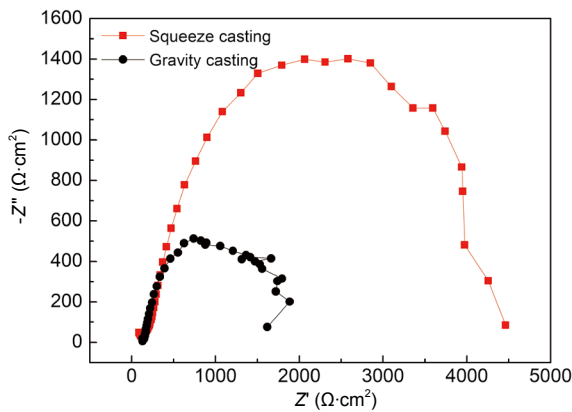


Fig. 11: EIS curves of WE43 alloy

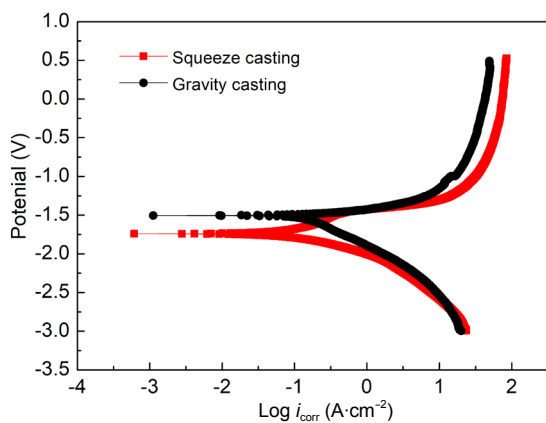


Fig. 12: PDP curves of WE43 alloy

4 Conclusions

(1) In the gravity cast WE43 alloy, the lamellar $\text{Mg}_{12}\text{Nd}_2\text{Y}$ phase is distributed along the grain boundary, and the grain distribution is uneven, the average grain size is $42 \mu\text{m}$. In squeeze cast WE43 alloy, many fine strips of the $\text{Mg}_{12}\text{Nd}_2\text{Y}$ phase form at the grain boundary, the grain size distribution is more concentrated, and the average grain size decreases to $36 \mu\text{m}$.

(2) The yield strength, tensile strength, and elongation of the gravity cast WE43 alloy are 127 MPa, 157 MPa, and 6%, and those of squeeze cast alloy are 145 MPa, 193 MPa, and 9.1%, which are obviously improved.

(3) The average corrosion rates of the gravity and squeeze cast WE43 alloys are 1.4135 and $0.6056 \text{ mm}\cdot\text{year}^{-1}$, respectively, according to the immersion test. The EIS and PDP curves show that the squeeze cast WE43 alloy has high corrosion resistance, and its corrosion current density is $78.13 \mu\text{A}\cdot\text{cm}^{-2}$.

Acknowledgements

The authors would like to acknowledge the State Key Project of Research and Development Plan of China (No. 2018YEB1106003), Dongguan Social Science and Technology Development Key Project (No. 2020507140148), Guangdong Provincial Key Laboratory of Advanced Forming of Light Metal Materials (No. 2021B1212050001) and Key-area Research and Development Program of Guangong Province (No. 2020B010186002) for supporting this research.

References

- [1] Zhang J, Huang H, Yang C B. Effects of hot ring forging on microstructure, texture and mechanical properties of AZ31 magnesium alloy. *Materials Science and Engineering A*, 2017, 679: 20–27.
- [2] Fu Y, Liu C, Hao H, et al. Effect of ageing treatment on microstructures, mechanical properties and corrosion behavior of Mg-Zn-RE-Zr alloy micro-alloyed with Ca and Sr. *China Foundry*, 2021, 18(2): 131–140.
- [3] Cui W D, Xiao L, Liu W C, et al. Effect of Zn addition on microstructure and mechanical properties of Mg-9Gd-3Y-0.5Zr alloy. *Journal of Materials Research*, 2018, 33(6): 733–744.
- [4] Li H X, Qin S K, Yang C L, et al. Influence of Ca addition on microstructure, mechanical properties and corrosion behavior of Mg-2Zn alloy. *China Foundry*, 2018, 15(5): 363–371.
- [5] Cihova M, Martinelli E, Schmutz P, et al. The role of zinc in the biocorrosion behavior of resorbable Mg-Zn-Ca alloys. *Acta Biomaterialia*, 2019, 100, 398–414.
- [6] Manne B, Thiruvayapati H, Bontha S, et al. Surface design of Mg-Zn alloy temporary orthopaedic implants: Tailoring wettability and biodegradability using laser surface melting. *Surface and Coatings Technology*, 2018, 347: 337–349.
- [7] Li N, Guo C, Wu Y H, et al. Comparative study on corrosion behaviour of pure Mg and WE43 alloy in static, stirring and flowing Hank's solution. *Corrosion Engineering Science and Technology*, 2012, 47(5): 346–351.
- [8] Levorova J, Duskova J, Drahos M, et al. In vivo study on biodegradable magnesium alloys: Bone healing around WE43 screws. *Journal of Biomaterials Applications*, 2018, 32(7): 886–895.
- [9] Dobatkin S, Martynenko N, Anisimova N, et al. Mechanical properties, biodegradation, and biocompatibility of ultrafine grained magnesium alloy WE43. *Materials*, 2019, 12(21): 3627.
- [10] Boland E L, Shirazi R N, Grogan J A, et al. Mechanical and corrosion testing of magnesium WE43 specimens for pitting corrosion model calibration. *Advanced Engineering Materials*, 2020, 20(10): 1800656.
- [11] Amani S, Faraji G. Recrystallization and mechanical properties of WE43 magnesium alloy processed via cyclic expansion extrusion. *International Journal of Minerals, Metallurgy, and Materials*, 2018, 25(6): 672–681.
- [12] Turkian A, Faraji G, Karimpour M. Mechanical properties and microstructure of WE43 Mg alloy processed by warm ECAP followed by extrusion. *Archives of Metallurgy and Materials*, 2018, 63(3): 1093–1100.
- [13] Kang Y H, Huang Z H, Zhao H, et al. Comparative study of hot deformation behavior and microstructure evolution of as-cast and extruded WE43 magnesium alloy. *Metals*, 2020, 10(4): 429.
- [14] Jahedi M, McWilliams B A, Knezevic M. Deformation and fracture mechanisms in WE43 magnesium-rare earth alloy fabricated by direct-chill casting and rolling. *Materials Science and Engineering A*, 2018, 726: 194–207.
- [15] Jahedi M, McWilliams B A, Moy P, et al. Deformation twinning in rolled WE43-T5 rare earth magnesium alloy: Influence on strain hardening and texture evolution. *Acta Materialia*, 2017, 131: 221–232.
- [16] Ghomashchi M R, Vikhrov A. Squeeze casting: An overview. *Journal of Materials Processing Technology*, 2000, 101(1): 1–9.
- [17] Li Y Y, Zhang W W, Zhao H D, et al. Research progress on squeeze casting in China. *China Foundry*, 2014, 11(4): 353–359.
- [18] You Z Y, Jiang A X, Duan Z Z, et al. Effect of heat treatment on microstructure and properties of semi-solid squeeze casting AZ91D. *China Foundry*, 2020, 17(3): 219–226.
- [19] Han Z Q, Pan H W, Li Y D, et al. Study on pressurized solidification behavior and microstructure characteristics of squeeze casting magnesium alloy AZ91D. *Metallurgical and Materials Transactions B*, 2015, 46(1): 328–336.
- [20] Wang B, Zhao Y H, Hou H. Study on microstructure and mechanical properties of Mg-xY-6xZn by squeeze casting. *Materials Research Express*, 2019, 6(6): 066574.
- [21] Jiang W M, Zhu J W, Li G Y, et al. Enhanced mechanical properties of 6082 aluminum alloy via SiC addition combined with squeeze casting. *Journal of Materials Science and Technology*, 2021, 88: 119–131.
- [22] Zhu J W, Jiang W M, Li G Y, et al. Microstructure and mechanical properties of SiC_{np}/Al6082 aluminum matrix composites prepared by squeeze casting combined with stir casting. *Journal of Materials Processing Technology*, 2020, 283: 116699.
- [23] Zeng R C, Sun L, Zheng Y F, et al. Corrosion and characterisation of dual phase Mg-Li-Ca alloy in Hank's solution: The influence of microstructural features. *Corrosion Science*, 2014, 79(2): 69–82.
- [24] Li T, He Y, Zhang H L, et al. Microstructure, mechanical property and in vitro biocorrosion behavior of single-phase biodegradable Mg-1.5Zn-0.6Zr alloy. *Journal of Magnesium and Alloys*, 2014, 2(2): 181–189.
- [25] Yang L, Huang Y, Feyerabend F, et al. Microstructure, mechanical and corrosion properties of Mg-Dy-Gd-Zr alloys for medical applications. *Acta Biomaterialia*, 2013, 9(10): 8499–8508.
- [26] Wei D, Wu S, Lue S, et al. Effects of rheo-squeeze casting parameters on microstructure and mechanical properties of AlCuMnTi alloy. *Materials Science and Engineering A*, 2012, 538: 320–326.
- [27] Gonor A L. High-pressure vaporization and boiling of condensed material: A generalized clausius-clapeyron equation. *AIP Conference Proceedings*, 2002, 620: 63–66.
- [28] Zhu S Z, Luo T J, Li Y J, et al. Characterization the role of squeezing pressure on microstructure, tensile properties and failure mode of a new Mg-6Zn-4Al-0.5Cu magnesium alloy. *Journal of Alloys and Compounds*, 2017, 718: 188–196.
- [29] Masoumi M, Hu H. Influence of applied pressure on microstructure and tensile properties of squeeze cast magnesium Mg-Al-Ca alloy. *Materials Science and Engineering A*, 2011, 528(10–11): 3589–3593.
- [30] Wang X Q, Cui F K, Yan G P, et al. Study on dislocation density change during cold roll-beating of 40Cr. *China Mechanical Engineering*, 2013, 24(16): 2248–2252.
- [31] Cai S H, Lei T, Li N F, et al. Effects of Zn on microstructure, mechanical properties and corrosion behavior of Mg-Zn alloys. *Materials Science and Engineering C*, 2012, 32: 2570–2577.
- [32] Baek S M, Kang J S, Shin H J, et al. Role of alloyed Y in improving the corrosion resistance of extruded Mg-Al-Ca-based alloy. *Corrosion Science*, 2017, 118: 227–232.
- [33] Walter R, Kannan M B. In-vitro degradation behaviour of WE54 magnesium alloy in simulated body fluid. *Materials Letters*, 2011, 65(4): 748–750.
- [34] Makar G L, Kruger J. Corrosion of magnesium. *International Materials Review*, 1993, 38(3): 138–153.
- [35] Cao F Z, Shi Z, Song G L, et al. Corrosion behaviour in salt spray and in 3.5% NaCl solution saturated with Mg(OH)₂ of as-cast and solution heat-treated binary Mg-X alloys: X=Mn, Sn, Ca, Zn, Al, Zr, Si, Sr. *Corrosion Science*, 2013, 76(11): 60–97.
- [36] Lai H Y, Li J Y, Li J X, et al. Effects of Sr on the microstructure, mechanical properties and corrosion behavior of Mg-2Zn-xSr alloys. *Journal of Materials Science-Materials in Medicine*, 2018, 29(6), 87.
- [37] Ralston K D, Fabijanic D, Birbilis N. Effect of grain size on corrosion of high purity aluminium. *Electrochimica Acta*, 2011, 56(4): 1729–1736.